DE GRUYTER OPEN

Acta Geophysica
vol. 63, no. 4, Aug. 2015, pp. 1044-1065
DOI: 10.1515/acgeo-2015-0029

3D Gravity Inversion using Tikhonov Regularization

Reza TOUSHMALANI[1] and Hakim SAIBI[2]

[1]Department of Computer, Faculty of Engineering, Kangavar Branch, Islamic Azad University, Kangavar, Iran; e-mail: geoman110@gmail.com

[2]Laboratory of Exploration Geophysics, Department of Earth Resources Engineering, Faculty of Engineering, Kyushu University, Fukuoka, Japan; e-mail: saibi-hakim@mine.kyushu-u.ac.jp (corresponding author)

Abstract

Subsalt exploration for oil and gas is attractive in regions where 3D seismic depth-migration to recover the geometry of a salt base is difficult. Additional information to reduce the ambiguity in seismic images would be beneficial. Gravity data often serve these purposes in the petroleum industry. In this paper, the authors present an algorithm for a gravity inversion based on Tikhonov regularization and an automatically regularized solution process. They examined the 3D Euler deconvolution to extract the best anomaly source depth as *a priori* information to invert the gravity data and provided a synthetic example. Finally, they applied the gravity inversion to recently obtained gravity data from the Bandar Charak (Hormozgan, Iran) to identify its subsurface density structure. Their model showed the 3D shape of salt dome in this region.

Key words: gravity inversion, base salt, Tikhonov regularization, Euler deconvolution, Bandar Charak.

1. INTRODUCTION

Subsalt exploration for oil and gas is attractive in regions where 3D seismic depth-migration to identify the geometry of the salt base is difficult. The complexity of the seismic ray paths and the lack of sufficient seismic energy

penetrating the salt make identifying the salt base difficult because of the complex shape of the salt and the high impedance contrast with the surrounding sediments. This problem may lead to poor imaging and inaccurate interpretations of subsalt geological structures. Additionally, 3D seismic data processing, particularly 3D seismic depth migration, which must be iteratively performed, is costly.

Additional information reduces the ambiguity in seismic images and helps speed up the iterative migration process. Model building would also be beneficial. Gravity data serve these purposes in the petroleum industry (Cheng 2003). The gravity method was the first geophysical technique, and it is used in oil and gas exploration. Despite being eclipsed by seismology, it has continued to be an important and sometimes crucial constraint in a number of exploration fields. In oil exploration, the gravity method is particularly applicable in salt provinces, over thrust and foothills belts, underexplored basins, and targets of interest that underlie high-velocity zones. The gravity method is frequently used in mining to map subsurface geology and to calculate reserves for some massive sulfide ore-bodies. In addition, there is a modest increase in the use of gravity techniques in specialized investigations for shallow targets, and these techniques are also applied in archeology, hydrogeology, and geothermal studies (Saibi *et al*. 2008). Data reduction, filtering, and visualization, together with low-cost, powerful personal computers and color graphics, have transformed the interpretation of gravity data. Euler and Werner deconvolution depth and edge estimation techniques can help define the lateral location and depth of isolated faults and boundaries from gravity data. Complex geology with overlapping anomalies arising from different depths can limit the effectiveness of deconvolution fault-detection results (Nabighian *et al*. 2005, Toushmalani 2011).

Mapping the Earth's structure in two and three dimensions is being addressed through various inverse techniques. Many researchers prefer inverse methods to forward modeling methods because they offer quantitative solutions that can be determined more often than the trial-and-error approach of forward modelling (Toushmalani and Saibi 2014).

Researchers are working on the inverse gravimetric problems to seek an operator to act on observed gravity data and return a subsurface density distribution that can generate the observed field. Li and Oldenburg (1998) presented a 3D inversion of gravity data and Li (2012) discussed the recent advances in 3D generalized inversion of potential-field data.

1.1 All types of operators

Some researchers assume a known density contrast and design nonlinear operators to determine the geometry of the source. Wavenumber domain meth-

ods have proven effective to determine the depth to a particular density interface, despite the difficulties associated with wavenumber domain transformations. These types of methods are less effective in determining full 3D solutions with multiple sources and varying density contrasts.

Other researchers use an approach similar to the one presented in this research. This approach solves the unknown density distribution by applying a linear operator to the data. Linear space domain operators are designed by fixing the geometry of the sources, usually by dividing the source volume into a number of elementary shapes, and allowing the density of the cells to vary. The linear approach is effective to determine the nature of small-scale geological features when given reasonable starting models. Recent advancements in computational power have made it feasible to use for regional problems as well.

The previously discussed methods are based on combining linear, spatial, and wavenumber domain calculations. These methods are strongly dependent on the variance of the initial model and advise users to run the program with different variances and initial models before making any geologic interpretation (Bear *et al*. 1995).

In this paper, the authors present an inverse method to derive objective 3D density distributions given map gravity data. The researchers used an appropriate estimate for the error on the right side, which can be determined automatically by projecting the rows of the matrix onto the "usable" rows of an orthogonalized version of the system based on the regularized solutions for an ill-conditioned system (Jones 2006).

It is difficult to obtain high-resolution images using a 3D gravity inversion, because the problem is extremely underdetermined (*i.e*., there are too many model parameters). To reduce the number of model parameters, a 3D gravity inversion scheme using Euler deconvolution as *a priori* information was proposed (Rim *et al*. 2007).

This paper is organized as follows: First, the Euler deconvolution method is described. Second, the "usable" rows of an orthogonalized version of the system based on regularized nonnegative solutions for an ill-conditioned system is discussed. Then, the techniques are applied to the solution of a general linear inverse problem. Finally, synthetic examples and a field data example are provided.

1.2 Euler deconvolution technique

Euler deconvolution is a technique that uses potential field derivatives to image the subsurface depth of a magnetic or gravity source (Thompson 1982, Hsu 2002). Mushayandebvu *et al*. (2001) described the 3D space Euler's deconvolution equation as

$$(x-x_0)\frac{\partial g}{\partial x}+(y-y_0)\frac{\partial g}{\partial y}+(z-z_0)\frac{\partial g}{\partial z}=-N\Delta g\ , \tag{1}$$

where (x_0, y_0, z_0) is the coordinate position of the top of the body, z is the depth measured (positive is downward), x is the horizontal distance, Δg is the value of the residual field, and N is a structural index. The structural index is a measure of the rate of change or fall off rate with the distance of a field. Therefore, it is a function of the geometry of the causative bodies. The magnetic field of a point dipole falls off with the inverse cube with an index of three, while a vertical line source gives an inverse square field fall off and an index of two. Extended bodies form assemblages of dipoles and will have indices ranging from zero to three (El Dawi *et al*. 2004, Reid *et al*. 1990).

If Δg_i is the residual gravity field at a point in a gravity survey, with the point measured at (x, y, z) and the coordinate position of the top of the body (x_0, y_0, z_0), then Eq. 1 can be written as

$$\begin{bmatrix}\frac{\partial \Delta g}{\partial x} & \frac{\partial \Delta g}{\partial y} & \frac{\partial \Delta g}{\partial z}\end{bmatrix}\begin{bmatrix}(x-x_0)\\(y-y_0)\\(z-z_0)\end{bmatrix}=-N\Delta gi\ . \tag{2}$$

By calculating the horizontal and vertical gradients of the field, Eq. 2 only has three unknowns x_0, y_0, z_0, and N. The first three describe the location of the body. Many simultaneous equations can be obtained for various measurement locations, which yield one matrix equation (Hansen and Suciu 2002).

$$\begin{bmatrix}\frac{\partial g^1}{\partial x} & \frac{\partial g^1}{\partial y} & \frac{\partial g^1}{\partial z}\\ . & & \\ . & & \\ \frac{\partial gi}{\partial x} & \frac{\partial gi}{\partial y} & \frac{\partial gi}{\partial z}\end{bmatrix}\begin{bmatrix}(x-x_0)\\(y-y_0)\\(z-z_0)\end{bmatrix}=N\begin{bmatrix}\Delta g^1\\.\\.\\.\\\Delta gi\end{bmatrix}. \tag{3}$$

The least squares method can be used to obtain the unknowns x_0, y_0, and z_0 if the structural index N is known. The Euler deconvolution method is used to estimate the depth and form of an anomaly, gravity and magnetic resources, the value of two factors of the Structural Index (SI) and the width of moving window size (W size). These values are sometimes determined by the interpreter using previous experience or regional geology, because they are not always clear. In this section, despite previous works, two loops were included in codes written in Matlab. In the first loop, all Structural Index (SI) values of sets of 0-3, with an increase of 0.5, were included. In the second

loop, moving window size (W size) odd values of 3-19 with an increase of 2 were included. All possible depths were extracted. Analyzing histograms of all z values showed that accepted values are the most frequent regarding the depth of model (Toushmalani and Hemati 2013).

2. METHODOLOGY

The authors addressed the gravimetric problem by assuming that the Earth can be represented by a finite number of rectangular blocks. This parameterization allows us to calculate the gravitational attraction caused by each block. The sum of the contributions from each of the individual blocks produces the observed gravity field (Fig. 1).

The gravity observed at any station (+) can be calculated by summing the contributions from each block at any point in question (Bear *et al*. 1995). The vertical gravitational attraction of a homogeneous body of an arbitrary shape can be shown as

$$g_z(x,y,z) = \gamma \int_{a1}^{a2}\int_{b1}^{b2}\int_{c1}^{c2} \frac{\rho c\,da\,db\,dc}{(a^2+b^2+c^2)^{3/2}} \ , \tag{4}$$

where

$$a_1 = u_1^i - x_i \ , \ a_2 = u_2^i - x_i \ , \ b_1 = v_1^i - y_i \ , b_2 = v_2^j - y_i \ , \ c_1 = w_1^j - z_i \ , \ c_2 = w_2^j - z_i \ ,$$

$g_z(x,y,z)$ is the vertical gravitational attraction at (x,y,z) resulting from the homogeneous body, γ is the universal gravitational constant, and ρ is the density of an elementary mass within the body. The location of the mass is (u, v, w). We evaluated Eq. 4 for a right rectangular prism. The integral can be expressed in elementary form as

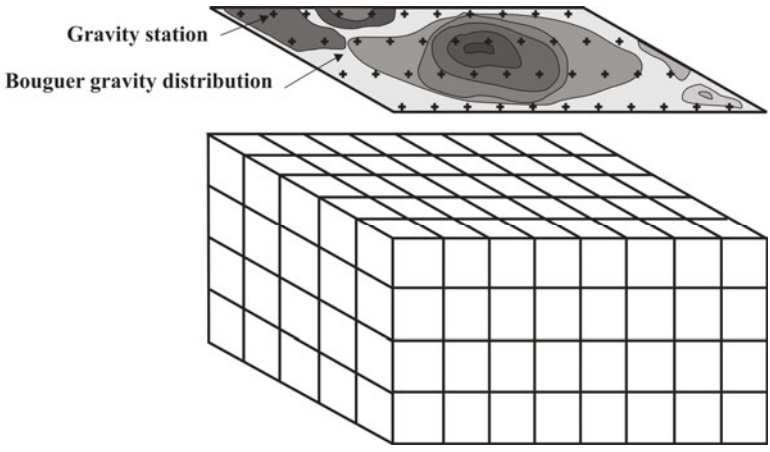

Fig. 1. Parameterization of the Earth model as rectangular blocks.

$$g_z = -\gamma\rho\left[x\ln\left(y+\left(x^2+y^2+z^2\right)^{\frac{1}{2}}\right)+ y\ln\left(x+\left(x^2+y^2+x^2\right)^{\frac{1}{2}}\right) + z\arctan\times z\left(\left(x^2+y^2+z^2\right)^{\frac{1}{2}}x^{-1}y^{-1}\right)\right] \begin{matrix} u_2^j - x_i \\ u_1^j - x_i \end{matrix}\Bigg]\begin{matrix} v_2^j - y_i \\ v_1^j - y_i \end{matrix}\Bigg]\begin{matrix} w_2^j - z_i \\ w_1^j - z_i \end{matrix} \tag{5}$$

and

$$A_{ij} = -\gamma\left[x\left|\ln\left(y+\left(x^2+y^2+z^2\right)^{\frac{1}{2}}\right)\right|+ y\left|\ln\left(x+\left(x^2+y^2+x^2\right)^{\frac{1}{2}}\right)\right| + z\arctan\times z\left(\left(x^2+y^2+z^2\right)^{\frac{1}{2}}x^{-1}y^{-1}\right)\right] \begin{matrix} u_2^j - x_i \\ u_1^j - x_i \end{matrix}\Bigg]\begin{matrix} v_2^j - y_i \\ v_1^j - y_i \end{matrix}\Bigg]\begin{matrix} w_2^j - z_i \\ w_1^j - z_i \end{matrix} \tag{6}$$

The edges of the *j* prism are parallel to the reference axes, and the limiting coordinates for its volume are u_1^j, u_2^j for the *x* coordinate, v_1^j, v_2^j for the *y* coordinate and w_1^j, w_2^j for the *z* coordinate (negative downward). The anomalous bodies responsible for observed gravity anomaly will be determined as a composition or accretion of prismatic cells with an assigned density contrast. Equation 5 is the product of the density of the block and a constant $\boldsymbol{A}_{ij}$ (the term in square brackets in Eq. 5), whose value is determined by the geometry of the block and its relation to the observation point. It is written as:

$$g_i = \sum_{j=1}^{m} A_{ij} P_j \ . \tag{7}$$

. The difference between the theoretical values calculated $\boldsymbol{g}_i^{\text{th}}$ from Eq. 5 and the observed gravity values $\boldsymbol{g}_i^{\text{obs}}$ at any observation point can be calculated. However, before this work:

- The gravity values calculated for initial density structure at points $\boldsymbol{\rho}_i$ are:

$$g_i^o = \sum_{j=1}^{m} A_{ij} P_j^o \ . \tag{8}$$

- In second step, a better model will be obtained by adding an additional density contrast $\Delta\boldsymbol{\rho}_j$ (maybe positive value $\Delta\boldsymbol{\rho}^+$ or maybe negative value $\Delta\boldsymbol{\rho}^-$) to the initial values $\boldsymbol{g}_i^o$.
- To obtain the final model, a linear regional trend is then adjusted

$$\delta_{gi} = g_{\text{obs}} - \left(g_i^o + A_{ij} \Delta\rho j \right) - \left(p_o + p_x x_i + p_y y_i \right) , \tag{9}$$

where p_o, p_x, and p_y are unknown simple regional trend (linear for instance) coefficients. In the next step,

$$\delta g_i = \sum_{j=1}^{m} A_{ij} \, \delta P_j \ . \tag{10}$$

The geometry of the sources remains fixed, so the geometric gravitational coefficients are constant ($\boldsymbol{A_{ij}}$) or n map observations and m prisms in the earth model. A system of linear equations can be formed as:

$$\begin{bmatrix} \delta_{g1} \\ \delta_{gn} \end{bmatrix} = \begin{bmatrix} a_{11} a_{12} a_{1m} \\ a_{n1} \quad a_{nm} \end{bmatrix} * \begin{bmatrix} \delta_{p1} \\ \delta_{pm} \end{bmatrix} . \tag{11}$$

The differential density is the only unknown in Eq. 11. The goal of the inversion is to estimate the differential density for each block (prism). Some researchers assumed a known density contrast and designed nonlinear operators to determine the geometry of the source. The wave number domain methods have proven effective to determine the depth to a particular density interface, despite the difficulties associated with wave number domain transformations. These types of methods are less effective in determining full 3D solutions with multiple sources and varying density contrasts. Other researchers used an approach similar to the one that is presented in this paper. This approach solves the unknown density distribution by applying a linear operator to the data. Linear space domain operators are designed by fixing the geometry of the sources, usually by dividing the source volume into a number of elementary shapes and allowing the density of the cells to vary.

The linear approach was effective in determining the nature of small-scale geological features when given a reasonable starting model. Recent advances in computational power have also made it feasible to use on regional problems. Methods are typically based on combining linear, spatial, and wave number domain calculations. These methods are strongly dependent on the variance of the initial model. Users are strongly advised to run the program with different variances and initial models before making any geologic interpretation (Bear *et al*. 1995).

Equation 11 can be rewritten in matrix form as:

$$\boldsymbol{g} = \boldsymbol{A}\,\boldsymbol{\rho} \ , \tag{12}$$

where $\boldsymbol{A}$ is an $n \times m$ matrix of geometrical coefficients, $\boldsymbol{g}$ is an n-length differential gravity vector, and $\boldsymbol{\rho}$ is an m-length vector of unknown perturbations.

$$
\begin{aligned}
&E = g_{\text{obs}} - g_{\text{cal}} = g_{\text{obs}} - Ap \Rightarrow e^2 = E^T E \\
&\Rightarrow e^2 = [g_{\text{obs}} - Ap]^T [g_{\text{obs}} - Ap] \\
&\Rightarrow e^2 = g_{\text{obs}}^T \quad g_{\text{obs}} - 2p^T A^T g_{\text{obs}} + p^T A^T Ap \\
&\text{minimization} \Rightarrow \frac{\partial e}{\partial p} = -2A^T g - 2A^T Ap \Rightarrow \Delta p = \left(A^T A\right)^{-1} A\Delta g \\
&\Rightarrow e^2 = E^T E + \lambda^2 p^T p \Rightarrow \Delta p = \left[A^T A + \lambda I\right] A^T E
\end{aligned}
\tag{13}
$$

When performing Tikhonov or similar types of regularization of ill-conditioned linear systems, a free parameter λ must be determined. Common techniques, such as using L-curves, are somewhat daunting for non-experts, and automated methods of choosing λ have not been widely applied. A given choice of λ implies a corresponding residual for the resulting regularized system. An appropriate residual is easily determined from the error level on the right side if that is known.

Software solutions available in various forms at www.rejonesconsulting.com solve this general linear problem:

$\boldsymbol{Ax} = \boldsymbol{b}$ (ordinary equations),
$\boldsymbol{Ex} == \boldsymbol{f}$ (equality constraints),
$\boldsymbol{Gx} \geq \boldsymbol{h}$ (inequality constraints),

where $\boldsymbol{A}$ has m rows and n columns; $\boldsymbol{Ax} = \boldsymbol{b}$ may be underdetermined, squared or over-determined (that is, $m < n$, $m = n$, or $m > n$); $\boldsymbol{Ax} = \boldsymbol{b}$ may be ill-conditioned and/or singular.

The SVD of $\boldsymbol{A}$ is $\boldsymbol{A} = \boldsymbol{USV}^{\boldsymbol{T}}$. In the absence of the small elements in S, the natural solution is $\boldsymbol{x} = \boldsymbol{VS}^{-1}\boldsymbol{UT}^{\boldsymbol{b}}$.

Applying the equality and inequality constraints are necessary because of the NNLS algorithm in Lawson, which is well known and will not be presented here.

The interesting part of the solution process is determining a regularization parameter to apply to the ordinary equations when they are ill-conditioned and no good error estimates are available for $\boldsymbol{b_i}$. We obtained the parameter λ to use when we add the following equations to the system $\boldsymbol{Ax} = \boldsymbol{b}$:

$$\boldsymbol{\lambda Ix} = 0 \ ,$$

where $\boldsymbol{I}$ is an identity matrix of size n by n.

Adding these equations is typically referred to as Tikhonov regularization. Determining a value for $\boldsymbol{\lambda}$ automatically (or even manually) is difficult. We found that this can be done by examining the Picard Condition Vector, or $\boldsymbol{p}$, where $\boldsymbol{V^T x} = \boldsymbol{S^+ U^T b} = \boldsymbol{p}$ ($\boldsymbol{S}^+$ is the same as $\boldsymbol{S}^{-1}$, except zero is used when $\boldsymbol{S_i}$ is zero).

The Discrete Picard Condition says that for a good solution, one should expect the coefficients in $\boldsymbol{p}$ to decline toward zero. In ill-conditioned problems, the Discrete Picard Condition is violated. We developed heuristics to detect where to pick the index in $\boldsymbol{p}$ to declare that the condition was violated. The number of elements of $\boldsymbol{p}$ before the rise was called the "usable rank" and was labeled $\boldsymbol{u}$. We then estimated the average error in $\boldsymbol{b}$ as follows: if $\boldsymbol{S}^{U}$ was the same as $\boldsymbol{S}^{-1}$, except for the rows beyond $\boldsymbol{i} = \boldsymbol{u}$, it was set to zero. We then computed $\boldsymbol{x}^{U}$, the more truncated SVD solution, for $\boldsymbol{x}$:

$$x^{U} = VS^{U}U^{T}b \ .$$

The residual vector $\boldsymbol{r}$ is then:

$$\boldsymbol{r} = \boldsymbol{A}\boldsymbol{x}^{U} - \boldsymbol{b}$$

and

$$\sigma = \sqrt{\frac{1}{m-u}\sum_{i-1}^{i-m} r_i^2} \ . \tag{14}$$

We estimated that the average error or standard deviation (σ) in the original $\boldsymbol{b_i}$ to be the root-mean-square of the elements of r. It is, however, divided by the number of unused rows, m-r, rather than by the number of elements, m. Next, λ is determined by applying the "discrepancy" method. λ is then adjusted until the solution to the regularized problem has the same norm of the residual vector as $\boldsymbol{x}^{U}$. The value of λ is then used to apply the equality and inequality constraints (Lawson and Hanson 1995). Geophysics articles and references divide the study area into a set of prisms (Pick *et al*. 1973), which are selected from the Bear article, but with a difference. In the majority of articles (possibly in all of the articles), the minimum and maximum depths are not clear. In this article, however, they were calculated using the Euler deconvolution method.

A code was written in MATLAB that receives data and divides it into a set of prisms, meaning that the desired area, $X_{\min}$ to $X_{\max}$, $Y_{\min}$ to $Y_{\max}$, and $Z_{\min}$ to $Z_{\max}$, is divided into a set of prisms with same dimensions. The number and dimensions of the prisms can be changed as desired. According to the MATLAB programming language, the area can be simply and quickly divided into 100 000 prisms. The linear operation in $\boldsymbol{g} = \boldsymbol{A}\boldsymbol{\rho}$ was used according to Bear *et al.* (1995). The solution of the equation is completed according to the Tikhonov and Lovenberg-Marqurdt methods, which determines the amount of λ. In this paper, the Autoreg method was applied to determine the most appropriate amount of λ. This was the first time this method was applied to solve a geophysics and gravity problem. By achieving the best λ and solving the previously discussed equation, the density contrast of all prisms was obtained.

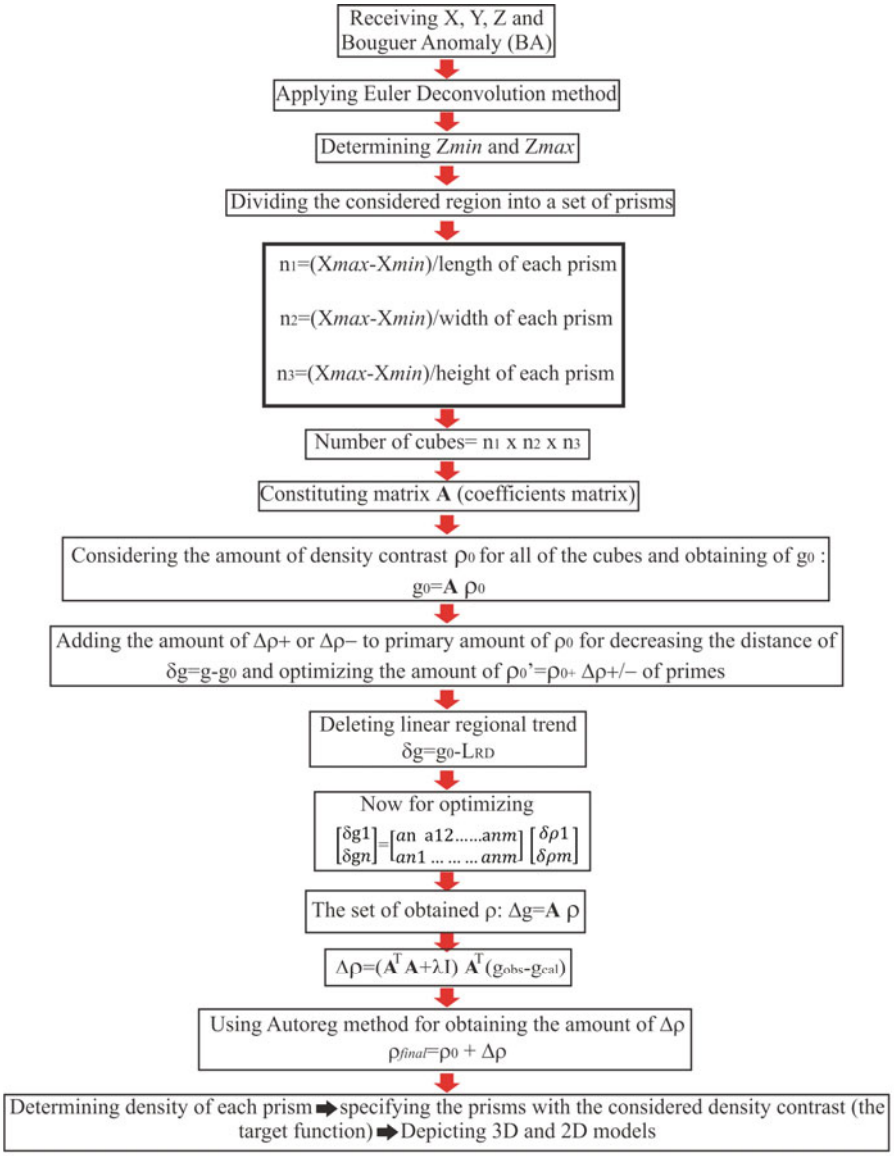

Fig. 2. The main flow chart of a 3D inversion algorithm of gravity data.

The next code section investigated the densities. After solving the equation using the previously mentioned methods for the code, the amount of a density contrast was obtained. The author looked for prisms with 400 density contrasts. After running the MATLAB code, the range of the cubes for the

study were specified. By devoting a trivial percent of error, 395 (minimum) and 405 (maximum), the differences can be determined. The code investigated all the prisms. The prisms with the discrepancy were then determined. They are depicted first in 3D diagram, and then in different 2D forms. Cubes of prisms with density discrepancies of –0.2 g/cm^3 were identified because the density of the region is between 2.3 g/cm^3, and the salt density is 2.1 g/cm^3. In this case, prisms with this density discrepancy are depicted. The flow chart of the methodology is shown in Fig. 2.

3. APPLICATION TO SYNTHETIC DATA

A buried anomalous structure is composed of two bodies that are characterized by a density contrast of 0.4 g/cm^3 with respect to the non-anomalous subsurface matter and, more or less, aligned along the X axis (Camacho *et al*. 2000, 2002, 2011). Figure 3 shows this structure. The anomalous masses and mass centers of these bodies are: body 1 with a mass of 264×10^{11} kg and a depth to its center $Z_1 = -134$ m and body 2 with a mass of 360×10^{11} kg and a depth to its center $Z_2 = -360$ m.

First, three-dimensional Euler deconvolution was applied to the model data. Most of the Euler solutions occurred in the vicinity of models (depth range between 0 to 500 m). The inversion constructed model spaces within a certain distance of the Euler solutions, and then searched systematically in those spaces.

The two L geometrical bodies with a positive density contrast of 0.4 g/cm^3 appear at different depths (Figs. 4-6).

First, we applied the 3D Euler deconvolution method to the synthetic model data. Most of the Euler solutions occurred in the vicinity of models with depths ranging between 0 and 500 m. Then, the model was divided into 960 prisms with dimensions of $200 \times 200 \times 50$ m in the x, y, and z directions, respectively.

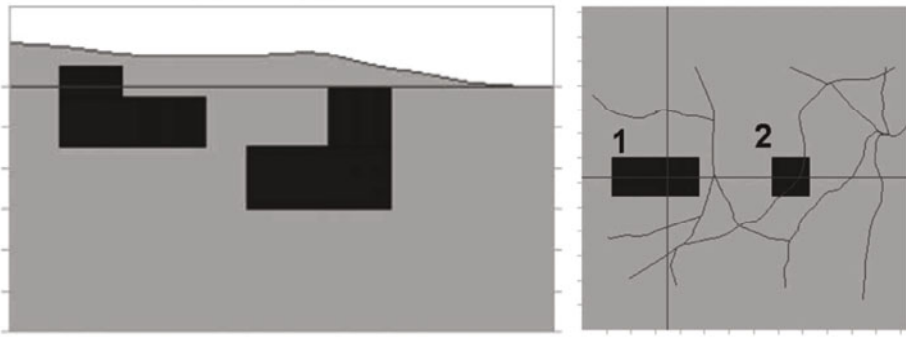

Fig. 3. Representation of original anomalous structures for first simulation test (Camacho *et al*. 2002).

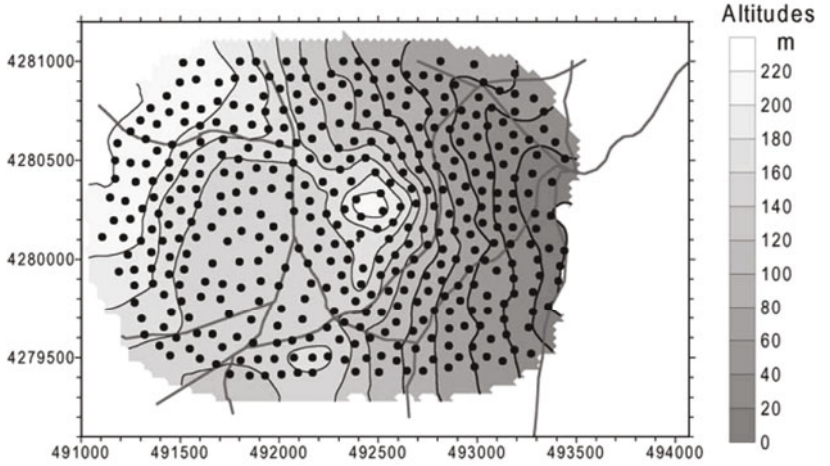

Fig. 4. Simulation example: contour map of altitudes ranging from 0 to 229 m and locations of 420 stations covering an area with a 2000 m diameter with a step of approximately 100 m (Camacho *et al*. 2002).

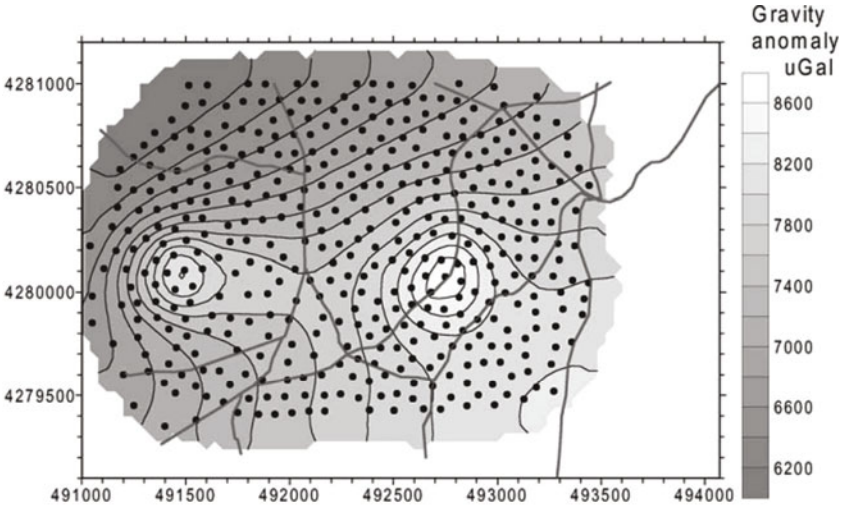

Fig. 5. Gravity anomaly due to anomalous bodies in Fig. 3 with anomalous density contrast of 0.4 g/cm^3 at the stations in Fig. 4 (Camacho *et al*. 2002).

Using the formula of Nagy *et al*. (2000), a coefficient matrix (prism gravity effect) was calculated, resulting in a 420×540 array matrix (being composed of 420 Bouguer anomaly measuring points and 540 prisms). Using the developed algorithm, all prisms with density contrasts of 0.4 g/cm^3 were obtained and are shown in Figs. 7 and 8. It is noticeable that if the in-

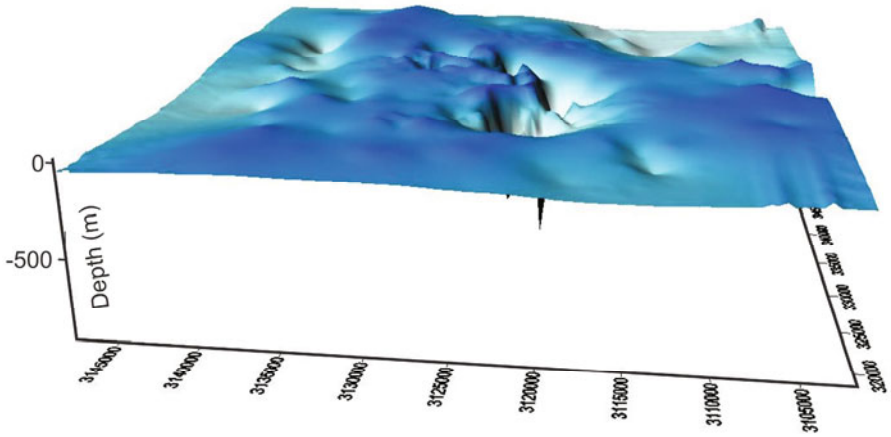

Fig. 6. 3D depth estimation of model with Euler deconvolution.

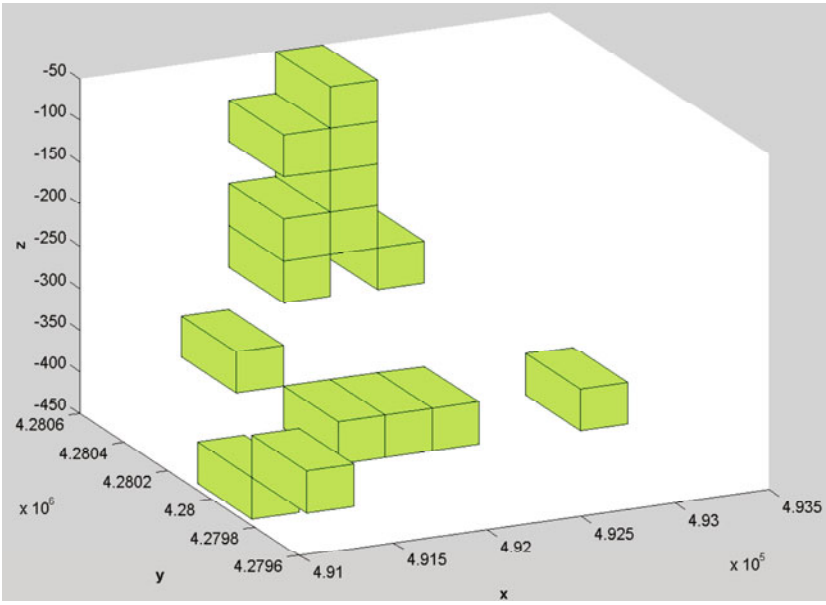

Fig. 7. 3D results of the inversion of gravity data from the synthetic model (green cubes represent prisms with a density contrast of 0.4 g/cm^3).

tended model is a combination of two or more objects with different density contrasts, we can do the search as many times as we wish using this method and depict the results each time in separate forms. Considering the intended model and the results achieved, this method can forecast the intended model with an acceptable rate; such a forecast includes the real depth and form of the anomaly source.

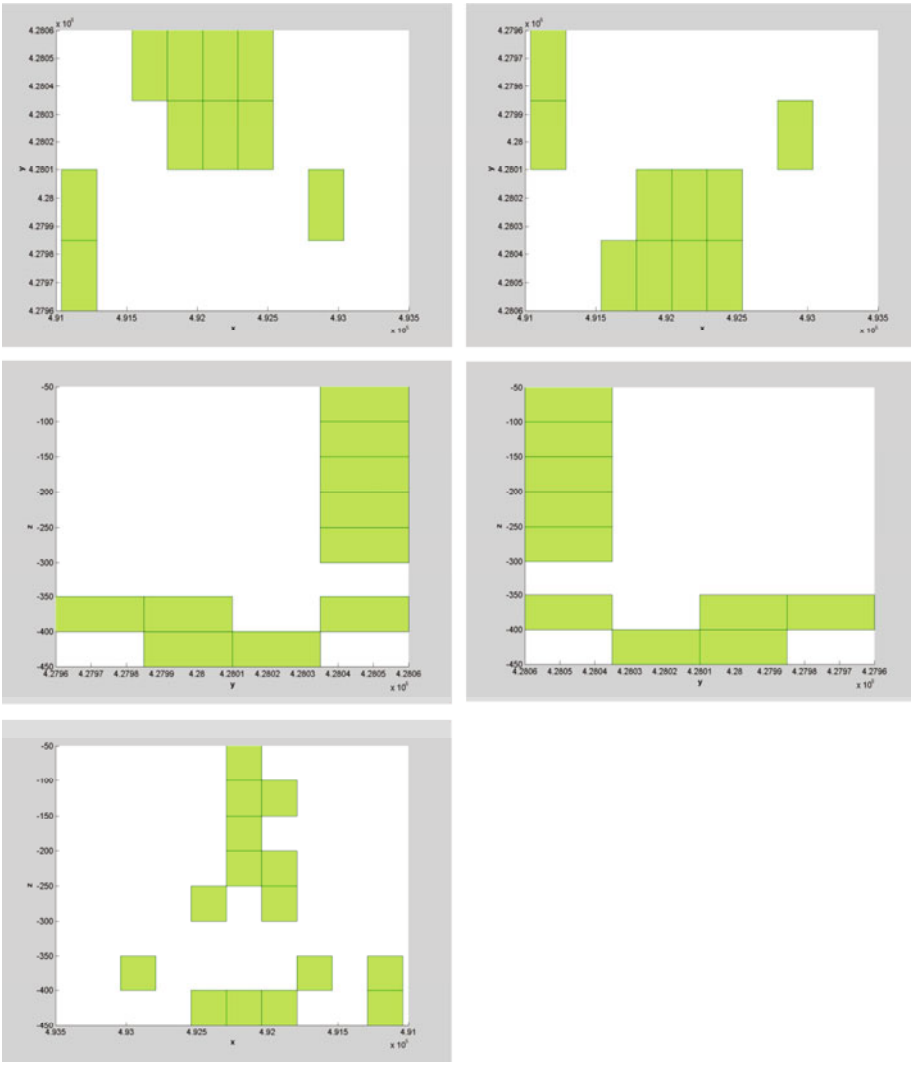

Fig. 8. All 2D views of the gravity inversion results from the synthetic model (green cubes represent prisms with a density contrast of 0.4 g/cm^3).

4. APPLICATION TO REAL GRAVITY DATA

The case study is the Bandar Charak (also known as Dehnow) region, located in southern Iran (Fig. 9a). A common method to determine the Bouguer density value as a random variable independent of topographic alternations was introduced by the Nettleton algorithm. During the correction processes, unexpected errors may occur. For example, the folded region of

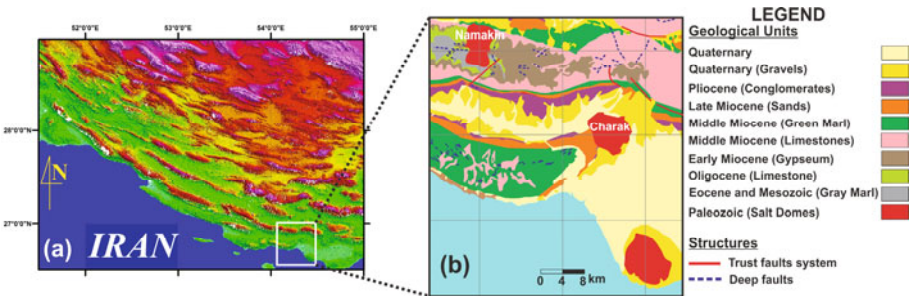

Fig. 9: (a) Elevation map from Shuttle Radar Topographic Mission (SRTM) data showing the location of the study area in Iran; and (b) geologic map of the study area.

Zagros is a result of crustal thickening processes in the southern regions ofIran. Sedimentary sequences in the Charak-Namakin anticlines are important geological units that have been selected for oil prospecting by the National Iranian Oil Company.

Gravimetric data sets were acquired at 776 stations by the National Iranian Oil Company through systematic land surveys. The main target areas along the Charak-Namakin salt domes are geographically located between 54.00-54.30 degrees longitude and 27.00-28.45 degrees latitude. Both the Asmari (Oligocene) and Pabdeh-Gurpi formations (early Cenozoic) contain limestones with gray marl intercalations, which is a potentially valuable facies for hosting hydrocarbon reservoirs under ascending movements of the Paleozoic formations in diapiric systems. The Hormoz series (Cambrian), containing gypsum and other related evaporates, traps oil volatiles that migrated to the nearby permeable brecciaed structures. The optimum Bouguer density is determined to only relate to the Charak geological impressions, which associates a number of gravimetric anomalies with the probable oil trap locations. This means that Bouguer anomalies are appropriate for density estimations using statistical techniques. The author applied this technique in the Bandar Charak (Hormozgan-Iran) with various geological/geophysical properties. These inversion results are comparable to both values obtained from density logs in the mentioned area and other methods, such as fractal methods.

The study area is surrounded by the cities of Ashkenan, Ahal, Boochir, Hamiran, Hashniz, and Kemeshck. The Tabnack gas structure is located to the west of this district. The area can be accessed through Asalouie (Bandar Lengeh, Lamard, and Ashkenan-Gavbandy roads) and has a very harsh topography with mountains and valleys. The climate is very hot and wet during the summer and average during the winter.

Geologically, Dehnow is a part of the Fars sedimentary basin in southeast Iran. Salt outcrops can be recognized at two points in the Dehnow anticline. The Khamy formation and Bangestan group are the oldest geological structures in the area that have outcrops. Younger structures are Aghajary, Mokhtari, Mishan, Gachsaran, and Asmary. Dominant structures trend northwest-southeast. The Dehnow anticline is located between the Hendurabi and Razak faults. These faults are almost perpendicular to the Dehnow anticline. Taking the combined geological-residual gravity contour map into account, the Dehnow anticline trends northwest-southeast.

A low gravity anomaly is located in the southeast of the anticline in the salt outcrop. A basic study of the geology of the area, a detailed investigation of the structural features (such as faults associated with the Dehnow anticline) and the application of geophysical techniques and other exploration methods is necessary to investigate the subsurface extension of this anticline and to identify the salt plug intrusion into the anticline. Gravity anomalies are the result of the interference among geological sources with different shapes, densities, and depths. Linear anomalies in geophysical maps, which may correspond to buried faults, contacts, and other tectonic and geological features, are particularly interesting for geologists. Most short-wavelength anomalies are caused by near-surface contacts of rocks that have density contrasts (Esmaeil Zadeh *et al.* 2010). Table 1 shows the density determination by sampling and system measurements in the Charak region, and Fig. 9b shows the geological map of Charak area.

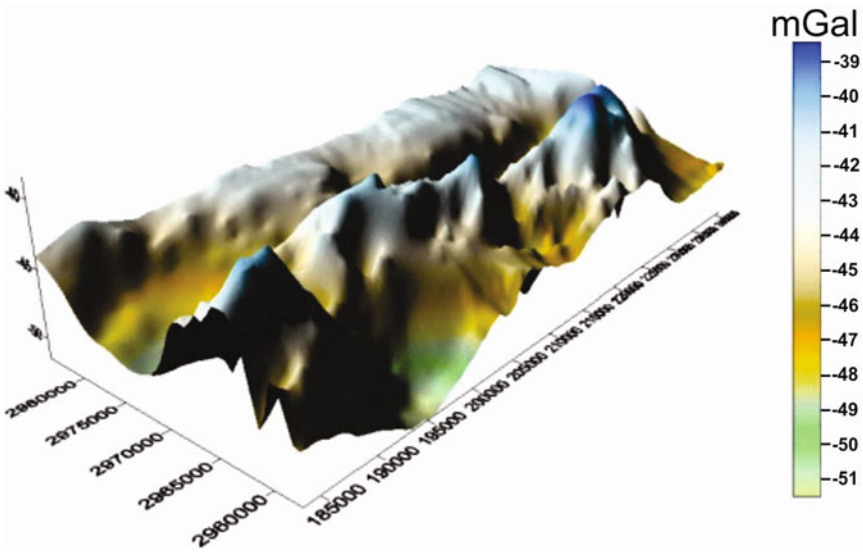

Fig. 10. Bouguer gravity map of the study area.

Table 1

Density determination by sampling and system measurements in the Charak region (National Oil Company of Iran, reported by Farmani 2003)

Sampling number	Coordinate [deg.]		Stratum	Lithology	Density [g/cm^3]
	Longitude [deg-min-s]	Latitude [deg-min-s]			
L18	54-36-48.2	26-31-48.6	Bakhtiari formation	Conglomerates and sandstone	1.87
L18					1.90
L18					1.90
L19					1.89
L19					1.86
L20	54-17-13.1	26-47-46	Mishan formation	Green marl	2.14
L20					2.12
L21					2.13
L22					2.07
L22					2.14
L23	54-16-57.4	26-48-5.9	Aghajari formation	Sandstone and marl	2.03
L24					2.02
L25					2.04
L26	53-38-17.8	27-5-2	Bangestan group	Limestone	2.45
L26					2.39
L27					2.41
L28					2.45
L29					2.39
L30	53-38-18.6	27-4-57.3			2.44
L31					2.43
L32					2.43
L35	53-37-43.3	27-4-18.3	Asmari – Gurpi formation	Limestone – gray marl	2.43
L36					2.45
L37					2.44
					2.36
					2.32
					2.32

Note: The mean density of the region is 2.3 g/cm^3.

The Bouguer gravity map of Bandar Charak region is presented in Fig. 10. The gravity anomalies range from –51.5 to –38.5 mGal. The 3D depth model of the study area is shown in Fig. 11. The 3D and 2D inversion results of the measured gravity data from the study region case using the developed algorithm are presented in Figs. 12 and 13, respectively.

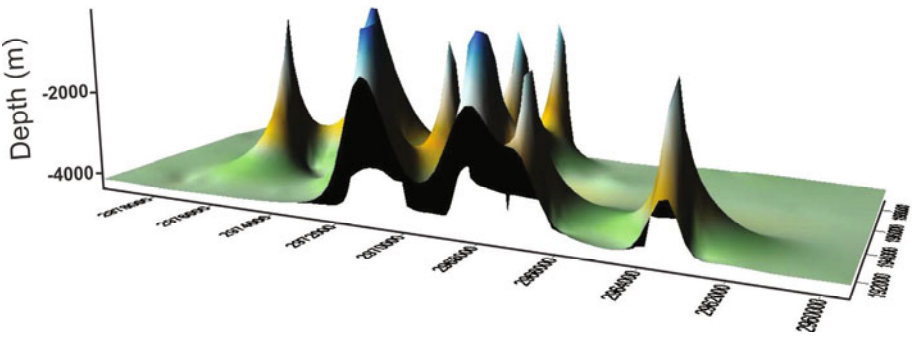

Fig. 11. 3D depth estimation with Euler deconvolution from the study area.

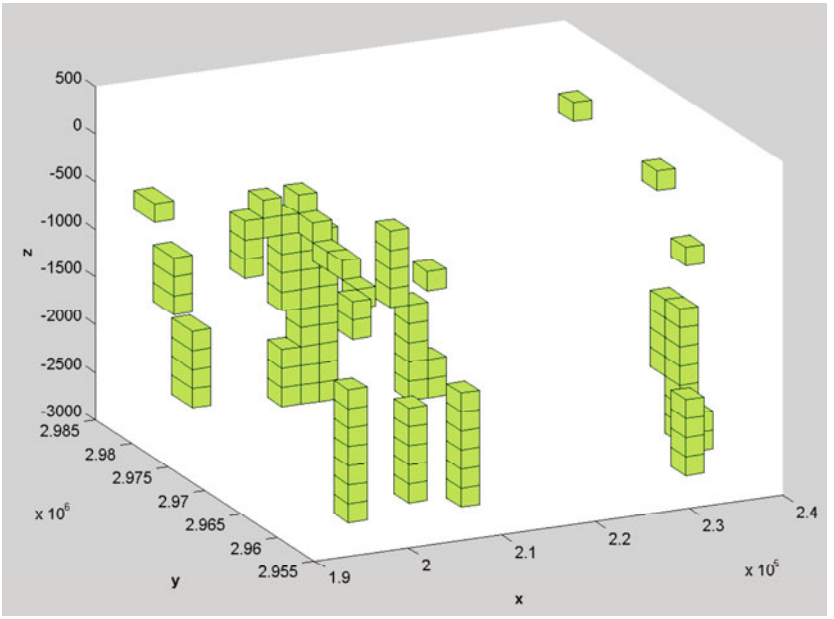

Fig. 12. 3D gravity inversion result of the case study area (green cubes represent prisms with a density contrast of –0.2 g/cm^3).

For the real case study, the minimum and maximum depths were calculated between zero and 4000 m using the Euler deconvolution method. Afterwards, the study area was divided into prisms with dimensions of $2000 \times 2000 \times 200$ m in the x, y, and z directions, respectively.

Using the developed 3D gravity inversion algorithm, all prisms with density contrasts of –0.2 g/cm^3 were detected and are shown in Figs. 12 and 13. In fact, prisms with such a density contrast are indicative of the figure of

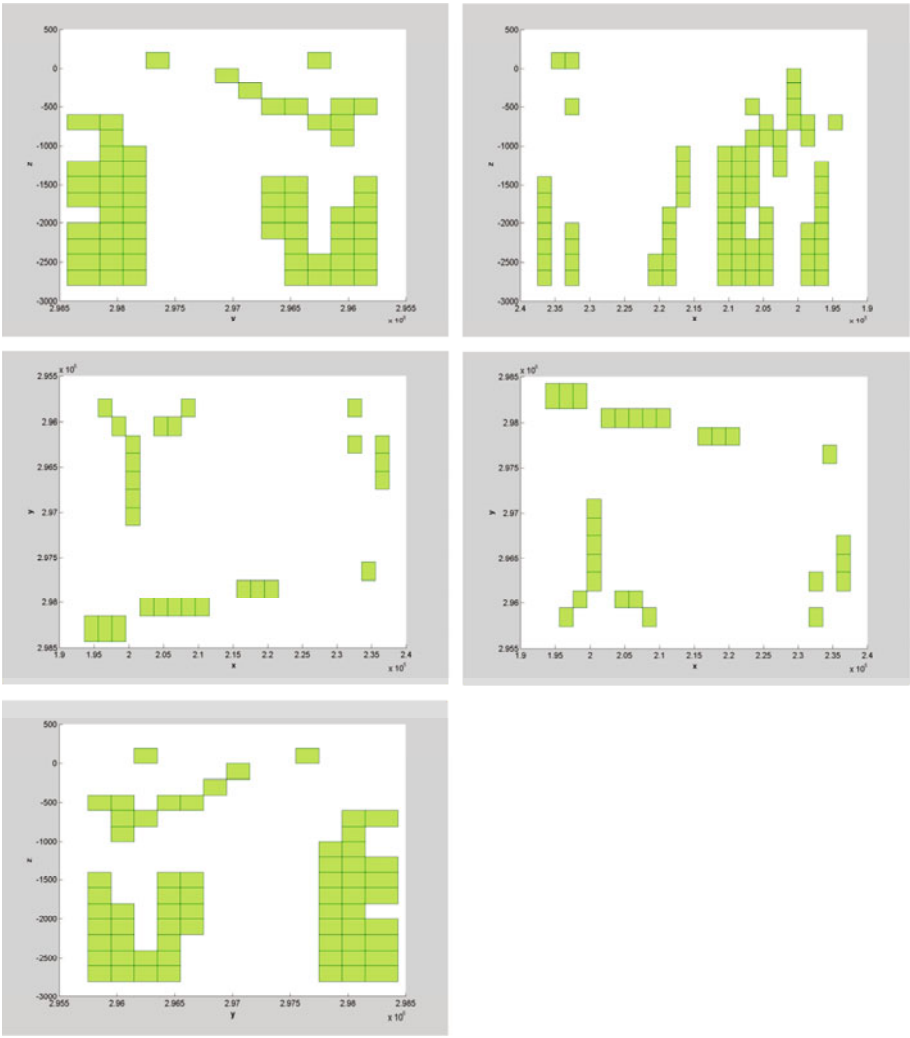

Fig. 13. All 2D results of the gravity inversion of the case study area (green cubes represent prisms with a density contrast of –0.2 g/cm^3).

the salt dome situated within the study area, making these results compatible with the research findings from geological (Bosak *et al*. 1998) and geophysical investigations (Esmaeil Zadeh *et al*. 2010) in the study area.

5. CONCLUSIONS

When performing Tikhonov's or similar types of regularization of ill-conditioned linear systems, a free parameter λ must be determined. A given choice of λ implies a corresponding residual for the resulting regularized sys-

tem. An appropriate residual is easily determined from the error level on the right side if it is known. This paper uses an estimate for the error on the right side that can be determined automatically by projecting the rows of the matrix onto the "usable" rows of an orthogonalized version of the system. Thus, the problem of picking λ is transformed into a problem of picking a "usable rank" at which to split the orthogonalized system. In this paper, the top of the salt and a part of the base of salt are not assumed to be accurately imaged. The densities of the background sediments, and thus the density contrast of the salt body, are assumed to be known. To estimate the depth of the top and bottom of the base of the salt, we used Euler deconvolution. We used this depth as *a priori* information in the inversion gravity procedure. Our 3D model shows the shape of the salt dome in this area.

References

Bear, G.W., H.J. Al-Shukri, and A.J. Rudman (1995), Linear inversion of gravity data for 3-D density distributions, *Geophysics* **60**, 5, 1354-1364, DOI: 10.1190/1.1443871.

Bosák, P., J. Jaroš, J. Spudil, and P. Sulovoský (1998), Salt plugs in the eastern Zagros, Iran: Results of regional geological reconnaissance, *Geolines* **7**, 1, 3-180.

Camacho, A.G., F.G. Montesinos, and R. Vieira (2000), Gravity inversion by means of growing bodies, *Geophysics* **65**, 1, 95-101, DOI: 10.1190/1.1444729.

Camacho, A.G., F.G. Montesinos, and R. Vieira (2002), A 3-D gravity inversion tool based on exploration of model possibilities, *Comput. Geosci.* **28**, 2, 191-204, DOI: 10.1016/S0098-3004(01)00039-5.

Camacho, A.G., J. Fernández, and J. Gottsmann (2011), The 3-D gravity inversion package GROWTH2.0 and its application to Tenerife Island, Spain, *Comput. Geosci.* **37**, 4, 621-633, DOI: 10.1016/j.cageo.2010.12.003.

Cheng, D. (2003), Inversion of gravity data for base salt, M.Sc. Thesis, Colorado School of Mines, Golden, USA, 95 pp.

El Dawi, M.G., T. Liu, H. Shi, and D. Luo (2004), Depth estimation of 2-D magnetic anomalous sources by using Euler deconvolution method, *Am. J. Appl. Sci.* **1**, 3, 209-214, DOI: 10.3844/ajassp.2004.209.214.

Esmaeil Zadeh, A., F. Doulati Ardejani, M. Ziaii, and M. Mohammado Khorasani (2010), Investigation of salt plugs intrusion into Dehnow anticline using image processing and geophysical magnetotelluric methods, *Russ. J. Earth Sci.* **11**, ES3008, DOI: 10.2205/2009ES000375.

Farmani, F. (2003), *Gravity Explorations Report in Namakin-Charak Region*, NIOC Press, 129 pp. (in Persian).

Hansen, R.O., and L. Suciu (2002), Multiple-source Euler deconvolution, *Geophysics* **67**, 2, 525-535, DOI: 10.1190/1.1468613.

Hsu, S-K. (2002), Imaging magnetic sources using Euler's equation, *Geophys. Prospect.* **50**, 1, 15-25, DOI: 10.1046/j.1365-2478.2001.00282.x.

Jones, R.E. (2006), Automatically regularized nonnegative solutions for ill-conditioned linear systems. **In:** *Proc. 2006 Inverse Problems in Engineering and Science Conf.*, 13 pp.

Lawson, C.L., and R.J. Hanson (1995), *Solving Least Squares Problems*, Classics in Applied Mathematics, Vol. 15, SIAM, Philadelphia, 337 pp., DOI: 10.1137/1.9781611971217.fm.

Li, Y. (2012), Recent advances in 3D generalized inversion of potential-field data. **In:** Proc. 82nd SEG Annual Meeting, 4-9 November 2012, Las Vegas, USA, Vol. 2, 878-884.

Li, Y., and D.W. Oldenburg (1998), 3-D inversion of gravity data, *Geophysics* **63**, 1, 109-119, DOI: 10.1190/1.1444302.

Mushayandebvu, M.F., P. van Driel, A.B. Reid, and J.D. Fairhead (2001), Magnetic source parameters of two-dimensional structures using extended Euler deconvolution, *Geophysics* **66**, 3, 814-823, DOI: 10.1190/1.1444971.

Nabighian, M.N., V.J.S. Grauch, R.O. Hansen, T.R. LaFehr, Y. Li, J.W. Peirce, J.D. Phillips, and M.E. Ruder (2005), The historical development of the magnetic method in exploration, *Geophysics* **70**, 6, 33ND-61ND, DOI: 10.1190/1.2133784.

Nagy, D., G. Papp, and J. Benedek (2000), The gravitational potential and its derivatives for the prism, *J. Geodesy* **74**, 7-8, 552-560, DOI: 10.1007/s001900000116.

Pick, M., J. Picha, and V. Vyskočil (1973), *Theory of the Earth's Gravity Field*, Elsevier, Amsterdam.

Reid, A.B., J.M. Allsop, H. Granser, A.J. Millett, and I.W. Somerton (1990), Magnetic interpretation in three dimensions using Euler deconvolution, *Geophysics* **55**, 1, 80-91, DOI: 10.1190/1.1442774.

Rim, H., Y.S. Park, M. Lim, S.B. Koo, and B.D. Kwon (2007), 3D gravity inversion with Euler deconvolution as a priori information, *Explor. Geophys.* **38**, 1, 44-49, DOI: 10.1071/EG07010.

Saibi, H., J. Nishijima, T. Hirano, Y. Fujimitsu, and S. Ehara (2008), Relation between structure and low-temperature geothermal systems in Fukuoka city, southwestern Japan, *Earth Planets Space* **60**, 8, 821-826, DOI: 10.1186/BF03352833.

Thompson, D.T. (1982), EULDPH: A new technique for making computer-assisted depth estimates from magnetic data, *Geophysics* **47**, 1, 31-37, DOI: 10.1190/1.1441278.

Toushmalani, R. (2011), Application of fuzzy c-means algorithm in Euler deconvolution depth optimization, *Int. J. Acad. Res.* **3**, 2, 44-48.

Toushmalani, R., and M. Hemati (2013), Euler deconvolution of 3D gravity data interpretation: New approach, *J. Appl. Sci. Agric*. **8**, 5, 696-700.

Toushmalani, R., and H. Saibi (2015), Fast 3D inversion of gravity data using Lanczos bidiagonalization method, *Arab. J. Geosci*. **8**, 7, 4969-4981, DOI: 10.1007/s12517-014-1534-4.

Received 3 February 2014
Received in revised form 1 September 2014
Accepted 26 September 2014